

Sliding-Rolling Ratio during Deep Squat with Regard to Different Knee Prostheses

Gusztáv Fekete¹, Patrick De Baets¹, Magd Abdel Wahab¹, Béla Csizmadia², Gábor Katona², Libardo V. Vanegas-Useche³, José Alfredo Solanilla³

¹ Ghent University, Laboratory Soete, Department of Mechanical Construction and Production, Ghent, Belgium, gusztav.fekete@ugent.be, patrick.debaets@ugent.be, magd.abdelwahab@ugent.be

² Szent István University, Institute of Mechanics and Machinery, Department of Mechanics and Technical Drawing, Gödöllő, Hungary, csizmadia.bela@gek.szie.hu, katona.gabor@gek.szie.hu

³ Technological University of Pereira, Faculty of Mechanical Engineering, Pereira, Colombia, lvanegas@utp.edu.co, joseing@utp.edu.co

Abstract: The sliding-rolling ratio between the femoral and tibial condyles throughout the active functional arc of the knee (20-120° of flexion angle) is currently unknown. Since wear is the most determining lifetime factor of the current total knee replacements, the presence of sliding-rolling cannot be neglected. The reason lies in the fact that this phenomenon causes different material abrasion compared to pure sliding or rolling alone. Only a limited amount of studies have dealt with this question related to the condyles of the knee prostheses, most of them by means of experimental tests and only in the segment where the motion begins (0 to 20-30°). The primary aim of this paper is to investigate how the sliding-rolling ratio changes between the condyles of five different knee prostheses in the functional arc of the knee (20-120°) as a function of flexion angle. For the analysis, five prosthesis models with identical boundary conditions have been constituted and numerical simulations were carried out using the MSC.ADAMS program system. Beside the sliding-rolling ratio, the normal and friction force between the connecting surfaces has also been calculated as a function of flexion angle.

Keywords: sliding-rolling ratio; contact forces; deep squat; knee prostheses

1 Introduction

In the case of normal flexion or extension of the human knee joint, the local kinematics of the patellofemoral joint can be characterized as partial rolling and sliding. This particular movement is under the control of the connecting femoral-

tibial surfaces and the connecting ligaments. The precise ratio of the sliding-rolling phenomenon throughout the active functional arc of the knee is currently unknown, although it is commonly accepted by the early works of Zuppinger [32] and Braune *et al.* [2] that up to 20-30° of flexion angle rolling is dominant, while beyond these angles the roles invert, and sliding becomes prevailing.

The combination of this complex motion, in addition to the incongruence of the connecting femoral and tibial condyles, raises the most difficult questions in the development of total knee replacements (later on TKRs). The relevance of the subject is undisputed, since during the knee or hip [17] prosthesis design, wear as an upcoming problem will appear in time. Only in the US, 350,000 total knee arthroplasty procedures are carried out annually [5], and it is shown in another study that for over the half of the retrieved prostheses failure is possibly due to wear or fatigue cracking [1].

Wear is the most determining lifetime factor in the current TKRs, and for this reason the presence of sliding-rolling cannot be neglected. The reason lies in the fact that this phenomenon causes different material abrasion compared to pure sliding or rolling alone [30]. Several test set-ups and techniques are available [14, 25, 29] to quantify the wear on the prosthesis surfaces, but it is only partially known what forces appear on the surface or how much sliding-rolling ratio should be applied during standard tests.

Besides the actual load, the sliding-rolling ratio is one of the most important parameters of the wear tests, since if it is set incorrectly high or low, then the wear will be over- or underestimated. There are only limited appearances in literature of numerical or analytical modeling of the sliding-rolling phenomenon, while experimental tests are slightly more frequent.

In regard to the experimental approaches, McGloughlin and Kavanagh [16] designed and built a three-station wear testing rig in order to assess the influence of kinematic conditions on the quantitative wear on the basis of TKR materials. In their study, they used a flat plate and a cylinder to measure how the wear rate is influenced by different sliding-rolling conditions. According to their results, above 50° of flexion angle at 0.95-0.99 sliding-rolling ratio, the wear rate reached the maximum. Reinholz *et al.* [24] developed a revolving simulator which allowed setting the sliding-rolling ratio between 0 to 1 (which means between 0 and 100% of sliding). In their experiments they investigated the alteration of the coefficient of friction up to 70% of sliding. Van Citters *et al.* [28] designed a six-station tribotester that is able to test six specimens simultaneously.

In their tests, the sliding-rolling ratio was set to a maximum 0.4 by means of creating 40% of sliding and 60% of rolling [27]. In other tests, Sukumaran *et al.* [26] applied a maximum of 0.3 sliding-rolling ratio.

In a comprehensive study, Hollman *et al.* [10] investigated the sliding-rolling behavior on 11 subjects without knee pathology and 7 subjects with injured

anterior cruciate ligaments. They proved with electromyographic signals and a mathematical model based on the concept of the path of instantaneous center of rotation (PICR) that the sliding-rolling coefficient varies between 0.3 and 0.46 in the early flexion angles (between 0 and 30°).

According to these studies, in the case of experimental testing of prosthesis materials, the sliding-rolling ratios are widely applied between 0.3-0.4 in the range of 0 to 30° flexion angle. Above this certain angle, only McGloughlin and Kavanagh [16] carried out experiments and proved that the sliding-rolling ratio reaches higher values, although they did not use real prosthesis components but rather a cylinder and a flat plate.

As for the numerical modeling side, one of the earliest models that investigated the sliding-rolling phenomenon is credited to Chittajallu and Kohrt [3]. In essence, their model is more like a stiffness model that considers all the major ligaments, but it can also calculate the sliding-rolling ratio. The ratio was defined as follows: a value of one represents pure rolling; infinite represents pure sliding; while intermediate values represent the combinations of the two phenomena. The major disadvantage in this model, besides the oversimplified surfaces (the femur is a circle, and the tibia plateau is a flat plate), is that the physical interpretation of the values between one and infinite is not clear.

On the basis of experiments carried out by Iwaki et al. [13] and Pinskerova et al. [22] on loaded, unloaded and cadaver knees, Nägerl et al. [21] re-investigated the question of the sliding-rolling ratio by analytical and numerical techniques and found new results in the higher range of flexion angle (Table 1).

Table 1

Various sliding-rolling ratios reported by Nägerl et al [21] based on the data of Pinskerova et al. [22]

Sliding-Rolling ratio	Range of flexion	Medial compartment			Lateral compartment		
		Loaded	Unloaded	Cadaver	Loaded	Unloaded	Cadaver
χ	0-20°	0.04	0.2	0.37	-0.24	0.83	0.63
χ	45-90°	0.9	0.91	0.92	0.8	0.57	0.57

It becomes apparent from Table 1 that the sliding-rolling ratio is slightly higher on the medial compartment than on the lateral compartment, and the loading condition alters the sliding-rolling ratio.

By summarizing the findings of the experimental and mathematical (numerical) literature, in the case of the experimental testing of prosthesis materials, the sliding-rolling ratios are widely applied between 0.3-0.46 [10, 26, 27, 28] but only in the range of 0 to 30° flexion angle due to the firm belief that in the beginning of the motion rolling is dominant. At higher flexion angles, presumably, the sliding-rolling ratio changes significantly [13, 16, 22], but the results related to the sliding-rolling ratio above 30° of flexion angle are rather limited.

Since the pattern of the sliding-rolling phenomenon has not been thoroughly investigated in full extension, the aims of this paper are:

- I To determine the pattern and magnitude of sliding-rolling ratio between 20-120° of flexion angle for several prosthesis geometries. This segment is considered as the fundamental active arc (see Figure 1) which is totally under muscular control and involves most of our daily activities [6]. For this reason, in this study the arcs between 0-20° and 120-160° are not considered.
- II To investigate how the sliding-rolling ratio changes depending on the different commercial and prototype prostheses. This should help to find the lower and upper limits of the sliding-rolling ratio between the condyles.
- III To investigate how the friction force and the normal force alter as a function of flexion angle with respect to realistic frictional condition. By knowing these forces in the active functional arc, the actual load during the wear test could be correctly set.

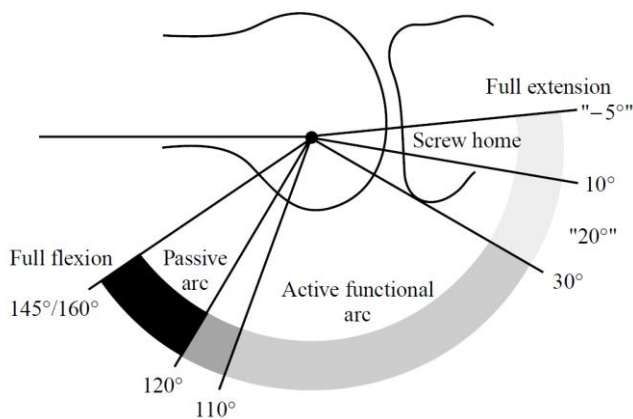


Figure 1

Major segments of human arc of flexion [21]

2 The Models

As a basis for the multibody models, several commercial prostheses and one prototype prosthesis were used. These prostheses are namely:

- Prosthesis 1: Prototype from the SZIU, non-commercial,
- Prosthesis 2: BioTech TP Primary knee [12],
- Prosthesis 3: BioTech TP P/S Primary knee [12],

- Prosthesis 4: BioMet Oxford Partial knee [11],
- Prosthesis 5: DePruy PFC [7].

The prostheses geometries were 3D scanned (Prost. 1-4) or received in STL files (Prost. 5). After correcting the disclosing errors of the surfaces by genetic algorithm [9] the geometries were converted into PARASOLID solid bodies.

2.1 Description of the Multibody Model

After creating the geometrical models, a multibody model was built in the MSC.ADAMS [20] program system. The following boundary conditions were applied on each model identically:

- The bones, such as the tibia, patella and femur, were assumed as rigid bodies, since the influence of deformation in this study is neglected.
- Only the patellar ligament and the quadriceps muscle were considered in the numerical model. The quadriceps muscle and the patellar ligament were modeled as simple linear springs (SPRING element see Figure 2). The stiffness coefficient was set to 130 N/mm and the damping coefficient to 0.15 Ns/mm for both springs, which correspond to the measured values in the literature [15, 18].
- A FORCE VECTOR was applied on the femur distalis (see Figure 2), which represented the load of the body weight (BW). The magnitude was set to 800 N (1 BW).
- The femur distalis was constrained by a GENERAL POINT MOTION, where all the coordinates can be prescribed (see Figure 2). Only one prescription was set: the endpoint of the femur (distalis) can only perform translational motion along the y axis.
- The ankle part of the model was constrained by a SPHERICAL JOINT, which allows rotation about all axes, but no translational motions are permitted at that point (see Figure 2). By applying this constraint, the tibia can perform a natural rotation and a kinematic analysis can be carried out in a further study.
- Between the femur, tibia and patella, CONTACT constraints were set according to Coulomb's law with respect to the very low static and dynamic friction coefficients ($\mu_s = 0.003$ $\mu_d = 0.001$) similarly to real joints [19, 23] (see Figure 2). The kinetic relationship between the normal and friction forces (F_n , F_s) and the flexion angle can be analyzed.

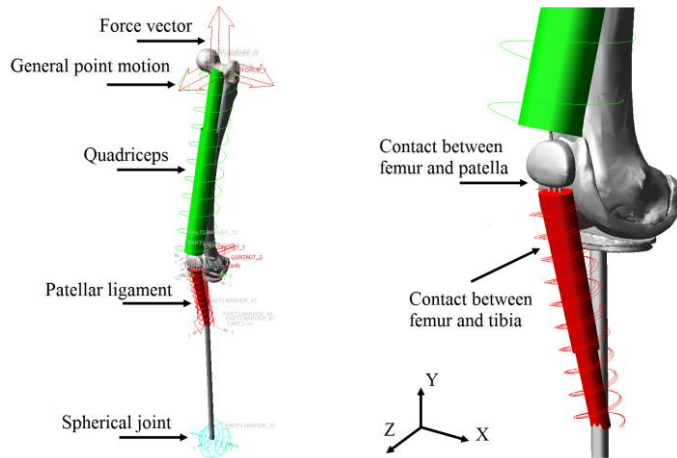


Figure 2
Multibody model

Since the MSC.ADAMS is a multibody dynamic program, it creates and solves simultaneously linear or non-linear Ordinary Differential Equations (ODE) and non-linear Differential-Algebraic Equations (DAE).

GSTIFF type integrator [8] was used in MSC.ADAMS for solving the ODE and DAE of the motion. The solver routine was set to work at a maximum 10^{-3} tolerance of error, while the maximum order of the polynomial was defined as 12. The solution converged very quickly with these parameters; the model in different positions during simulation is presented in Figure 3.

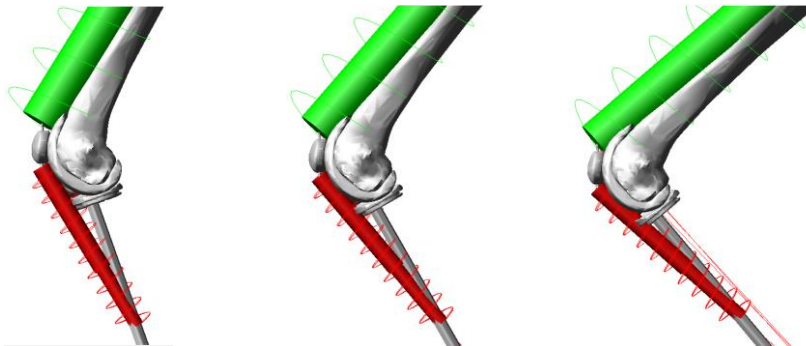


Figure 3
Multibody model in different positions during simulation

The post-processing was carried out in MSC.ADAMS and partly in Excel. The MSC.ADAMS software can directly compute forces, velocities and accelerations, but not rotations.

2.2 The Calculation Method

The following kinematic quantities can be directly calculated by MSC.ADAMS during the simulation of the motion as a function of time:

- $\bar{r}_{Ci}(t)$ vector-scalar function, which determines the instantaneous position of the connecting points of the two bodies defined in the absolute coordinate system (see Figure 4). If $i = 1$, contact between femur and tibia, if $i = 2$, contact between femur and patella.
- $\bar{r}_{CMF}(t)$, $\bar{r}_{CMT}(t)$, $\bar{v}_{CMF}(t)$, $\bar{v}_{CMT}(t)$, $\bar{\omega}_{CMF}(t)$ and $\bar{\omega}_{CMT}(t)$ vector-scalar functions, which determine the instantaneous position of the center of mass (CM_i), velocity and angular velocity of the femur (F) and the tibia (T) defined in the absolute coordinate system (see Figure 4).
- $\bar{e}_{Ci}(t)$ vector-scalar function (unit-vector), which determines the instantaneous tangent vector respectively to the contact path defined in the absolute coordinate system (see Figure 5).

Besides the kinematic quantities, the MSC.ADAMS software can calculate kinetic quantities as well, for example:

- Contact forces between the articular surfaces, reaction forces and moments in the applied constrains or forces in the springs.

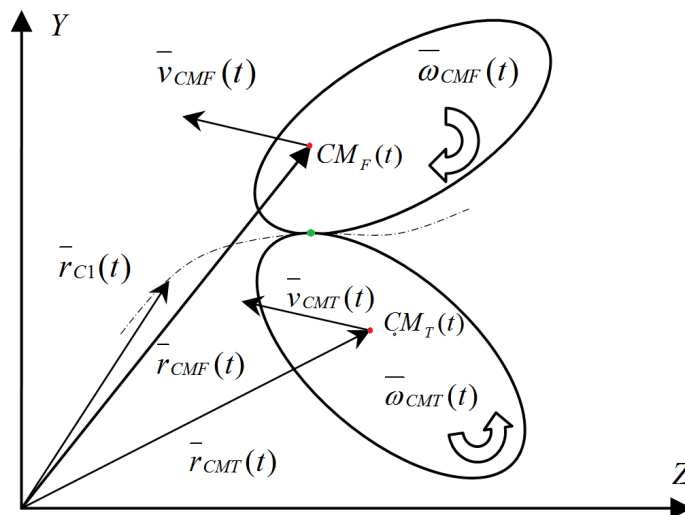


Figure 4

Kinematic quantities between the femur and tibia

In order to calculate the sliding-rolling ratio, additional kinematic quantities have to be determined as well (these quantities cannot be calculated directly with MSC.ADAMS):

- $\bar{r}_{CF}(t)$, $\bar{r}_{CT}(t)$, $\bar{v}_{CF}(t)$ and $\bar{v}_{CT}(t)$ are vector-scalar functions, which determine the instantaneous position and velocity in the contact point (C) of the connecting femoral or tibial surfaces respectively (see Figure 5).

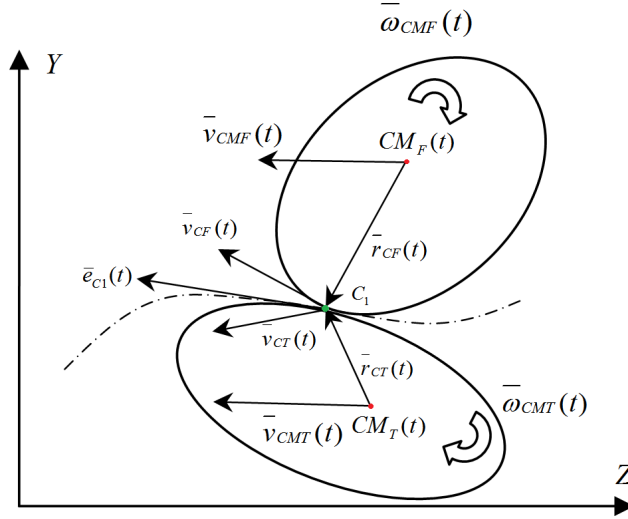


Figure 5

Kinematic quantities between the femur and tibia

Since the multibody model is considered rigid, the rigid body kinematics is applicable. To obtain the velocity of a point – in our case point C – the following calculation algorithm is as follows [4]:

$$\bar{v}_{CF}(t) = \bar{v}_{CMF}(t) + \bar{\omega}_{CMF}(t) \times \bar{r}_{CF}(t) \quad (1)$$

$$\bar{v}_{CT}(t) = \bar{v}_{CMT}(t) + \bar{\omega}_{CMT}(t) \times \bar{r}_{CT}(t) \quad (2)$$

where,

$$\bar{r}_{C1}(t) = \bar{r}_{CMF}(t) + \bar{r}_{CF}(t) \rightarrow \bar{r}_{CF}(t) = \bar{r}_{C1}(t) - \bar{r}_{CMF}(t) \quad (3)$$

$$\bar{r}_{C1}(t) = \bar{r}_{CMT}(t) + \bar{r}_{CT}(t) \rightarrow \bar{r}_{CT}(t) = \bar{r}_{C1}(t) - \bar{r}_{CMT}(t) \quad (4)$$

by substituting equation (3) and (4) into (1) and (2) we obtain,

$$\bar{v}_{CF}(t) = \bar{v}_{CMF}(t) + \bar{\omega}_{CMF}(t) \times (\bar{r}_{C1}(t) - \bar{r}_{CMF}(t)) \quad (5)$$

$$\bar{v}_{CT}(t) = \bar{v}_{CMT}(t) + \bar{\omega}_{CMT}(t) \times (\bar{r}_{C1}(t) - \bar{r}_{CMT}(t)) \quad (6)$$

Now, the velocities with respect to the femur and tibia are determined in the contact point, in the absolute coordinate system (see Figure 6).

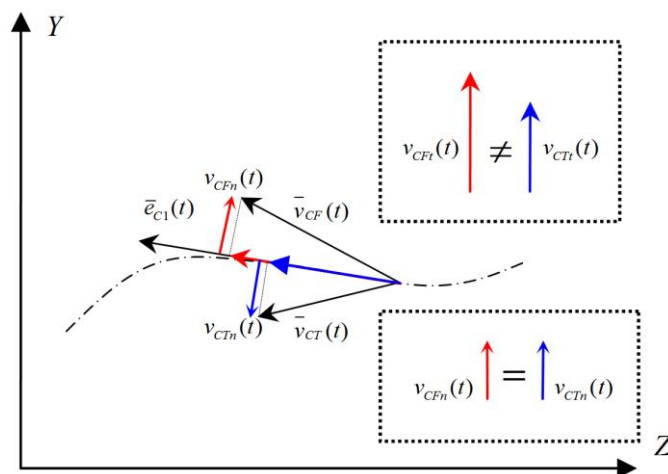


Figure 6

Velocities of the femur and tibia in the contact point

By multiplying equation (5) and (6) with the $\bar{e}_{C1}(t)$ unit vector, we can derive the tangential scalar component of the femoral and tibial contact velocities with respect to the contact path:

$$v_{CFt}(t) = [\bar{v}_{CMF}(t) + \bar{\omega}_{CMF}(t) \times (\bar{r}_{C1}(t) - \bar{r}_{CMF}(t))] \cdot \bar{e}_{C1}(t) \quad (7)$$

$$v_{CTt}(t) = [\bar{v}_{CMT}(t) + \bar{\omega}_{CMT}(t) \times (\bar{r}_{C1}(t) - \bar{r}_{CMT}(t))] \cdot \bar{e}_{C1}(t) \quad (8)$$

The tangential scalar components are only valid, if the following condition is satisfied:

$$v_{CFn}(t) = v_{CTn}(t) \quad (9)$$

This means that the normal scalar components of the femoral and tibial contact velocities must be equal; otherwise the two surfaces would be either crushed into each other or would be separated.

Since scalar contact velocities are available, by integrating them over time the connecting arc lengths with respect to the femur and tibia can be calculated as:

$$S_{femur}(t) = \int v_{CFt}(t) \cdot dt = \int [\bar{v}_{CMF}(t) + \bar{\omega}_{CMF}(t) \times (\bar{r}_{C1}(t) - \bar{r}_{CMF}(t))] \cdot \bar{e}_{C1}(t) \cdot dt \quad (10)$$

$$S_{tibia}(t) = \int v_{CTt}(t) \cdot dt = \int [\bar{v}_{CMT}(t) + \bar{\omega}_{CMT}(t) \times (\bar{r}_{C1}(t) - \bar{r}_{CMT}(t))] \cdot \bar{e}_{C1}(t) \cdot dt \quad (11)$$

By having the arc lengths on both connecting bodies, the sliding-rolling ratio can be introduced, and denoted by χ :

$$\chi(t) = \frac{\Delta S_{tibiaN}(t) - \Delta S_{femurN}(t)}{\Delta S_{tibiaN}(t)} \quad (12)$$

where,

$$\Delta S_{femurN}(t) = S_{femurN}(t) - S_{femurN-1}(t) \quad (13)$$

$$\Delta S_{tibiaN}(t) = S_{tibiaN}(t) - S_{tibiaN-1}(t) \quad (14)$$

are the corresponding incremental differences of the connecting arc lengths.

The χ function – or sliding-rolling function – is defined as the ratio of the distance travelled by the contact point on the tibia to the distance travelled by the contact point on the femur over a specified increment of movement. By this function, exact conclusions can be drawn about the sliding and rolling features of the motion. A sliding-rolling ratio (χ) of zero indicates pure rolling, while one describes pure sliding. If the ratio is between zero and one, the movement is characterized as partial rolling and sliding. For example a sliding-rolling ratio of 0.4 means 40% of sliding and 60% of rolling. A positive ratio shows the slip of the femur compared to the tibia. If the sign is negative, then the tibia has higher slip compared to the femur.

It is desirable to determine the sliding-rolling ratio as a function of flexion angle rather than the time; thus the flexion angle (α) was derived by integrating the angular velocities of the femur and tibia about the x axis over time, and taking this into account, the model was set in an initial 20 degree of squat at the beginning of the motion.

$$\alpha(t) = \int \omega_{CMFx} \cdot dt + \int \omega_{CMTx} \cdot dt + 20 \quad (15)$$

Since the $\alpha(t)$ function has been determined, the time can be exchanged to flexion angle and the sliding-rolling function (χ) can be plotted as a function of flexion angle:

$$\chi(\alpha) = \frac{\Delta S_{tibiaN}(\alpha) - \Delta S_{femurN}(\alpha)}{\Delta S_{tibiaN}(\alpha)} \quad (16)$$

3 Results

After all of the simulations were carried out on all the five prostheses, the following results related to the sliding-rolling ratio and the connecting forces were obtained:

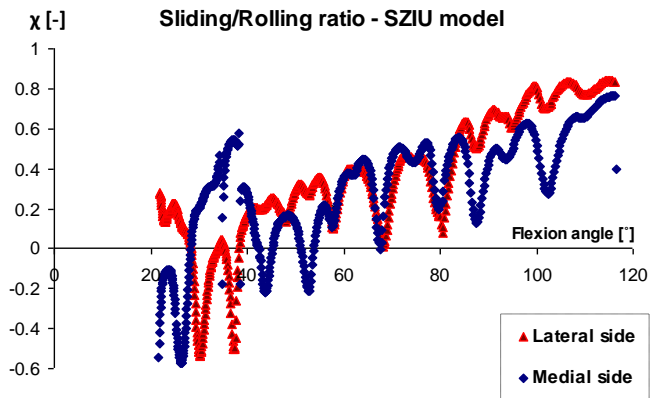


Figure 7
Sliding-rolling function of the SZIE model

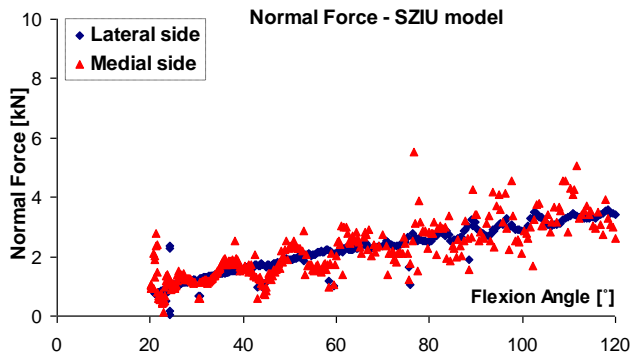


Figure 8
Normal force function of the SZIE model

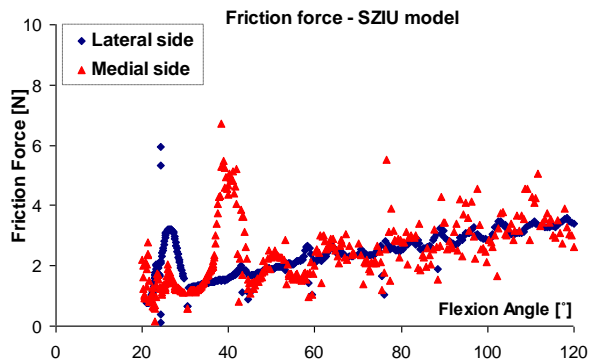


Figure 9
Friction force function of the SZIE model

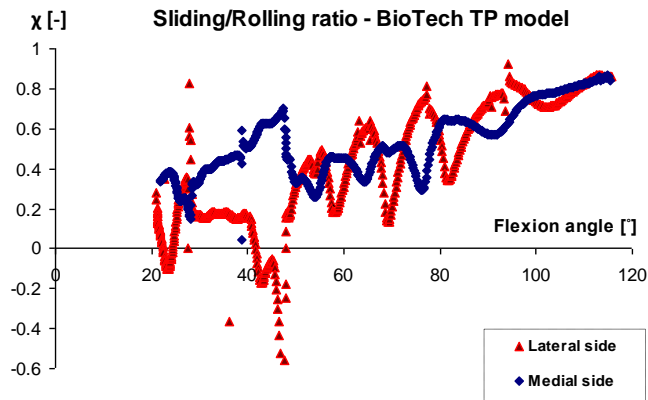


Figure 10

Sliding-rolling function of the BioTech TP model

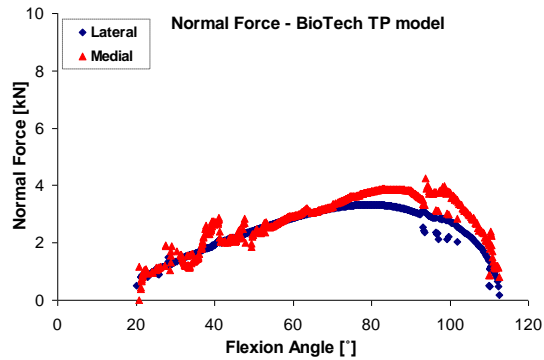


Figure 11

Normal force function of the BioTech TP model

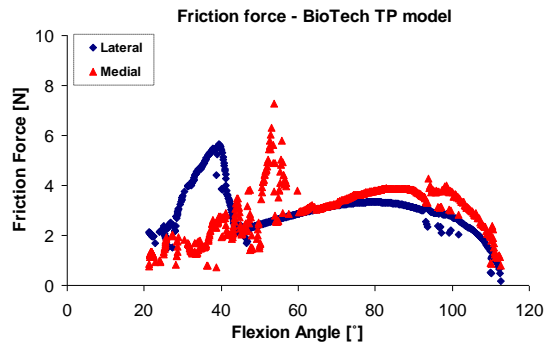


Figure 12

Friction force function of the BioTech TP model

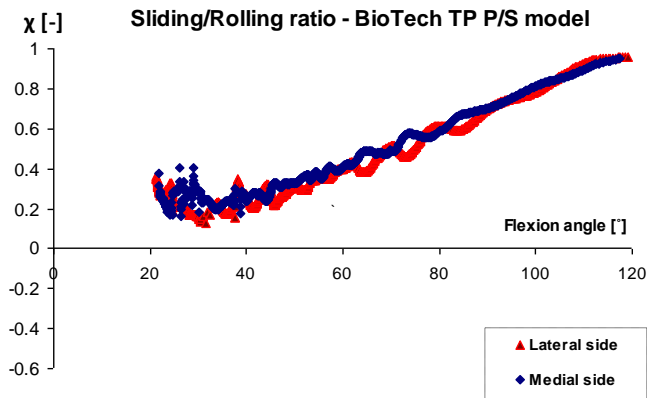


Figure 13
Sliding-rolling function of the BioTech TP P/S model

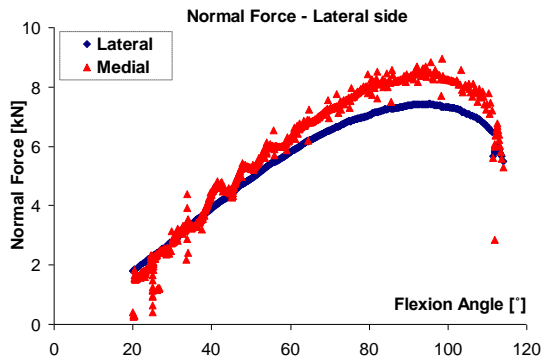


Figure 14
Normal force function of the BioTech TP P/S model

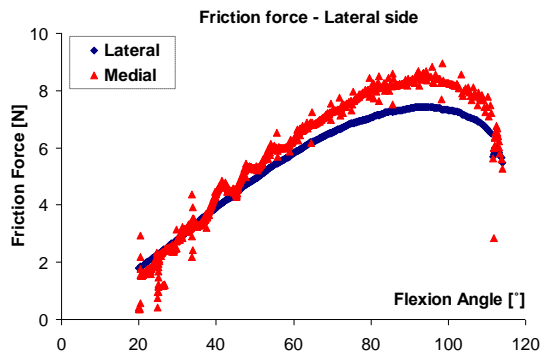


Figure 15
Friction force function of the BioTech TP P/S model

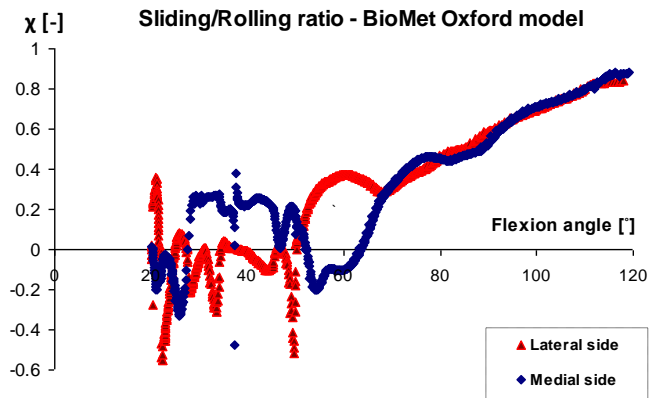


Figure 16

Sliding-rolling function of the BioMet Oxford model

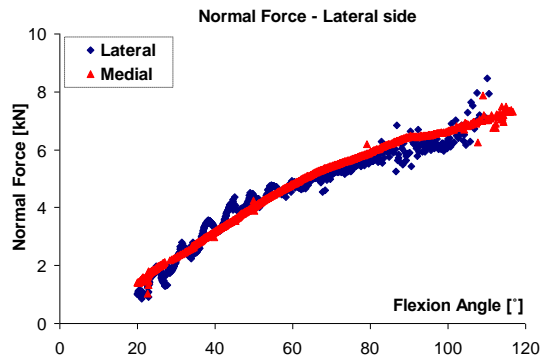


Figure 17

Normal force function of the BioMet Oxford model

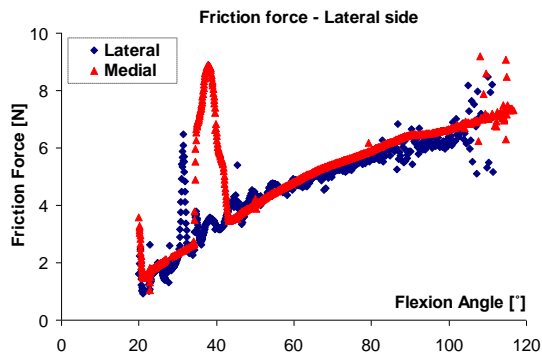


Figure 18

Friction force function of the BioMet Oxford model

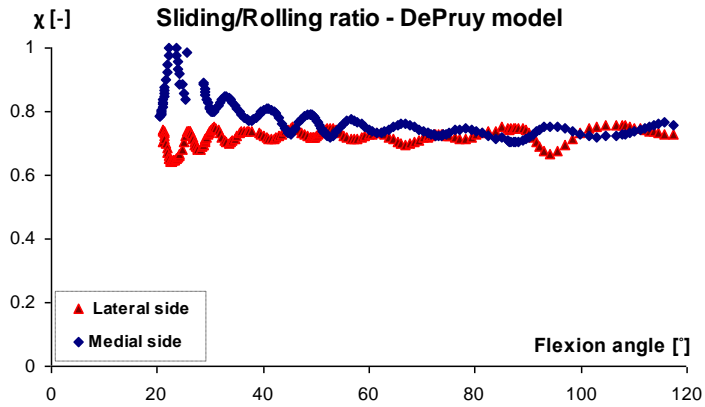


Figure 19
Sliding-rolling function of the DePruy model

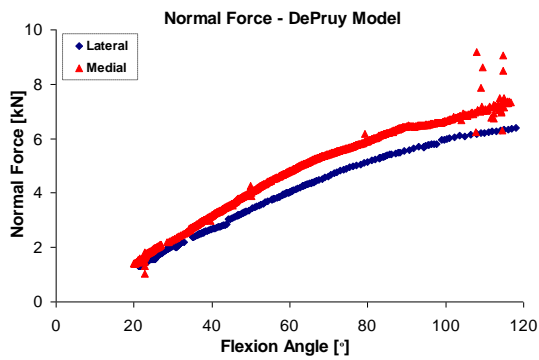


Figure 20
Normal force function of the DePruy model

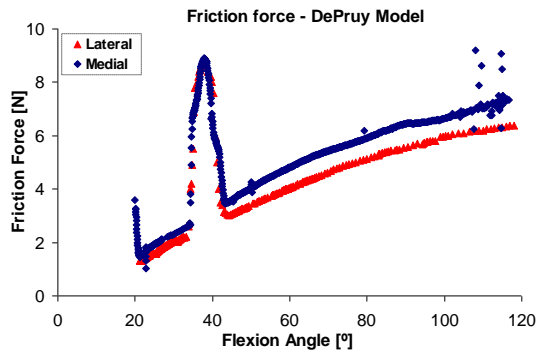


Figure 21
Friction force function of the DePruy model

Let us first look at the magnitude and the pattern of the sliding-rolling ratio of the different prostheses and then at the normal and friction forces.

In the case of the SZIU prototype model (Figure 7), the lateral side starts from a positive sliding-rolling ratio of 0.2, while the medial side starts between -0.25 and -0.6. Starting from 45° of flexion angle, the ratio increases with occasional irregularity to 0.86 in the lateral side and 0.76 in the medial side. If we neglect the occasional irregularity, the increment shows closely linear growth. With regard to the kinetics – namely the normal and friction force (Figures 8 and 9) – between the condyles, the evolution of the forces can be described as linearly increasing, with a maximum of 3.58 kN and 3.58 N with respect to the normal and the friction force. Generally more scatter is observed at the medial side.

The BioTech TP and the TP P/S models (Figures 10 and 13) are from the same manufacturer, although they have different characteristics both in their kinematics and kinetics. While the TP P/S model has a very smooth sliding-rolling evolution along the complete segment (0 to 120°), the normal and friction forces (see Figures 11 and 12) are twice as great compared to forces of the TP model (see Figures 14 and 15), where the sliding-rolling function is more hectic. The sliding-rolling curves of the TP start approximately from 0.4, while the TP P/S from 0.3. From 45-50° degree of flexion angle, both TP and TP P/S functions begin to increase, the TP P/S with much less irregularity. The maximum sliding-rolling ratio reaches 0.86 in the case of the TP model and 0.95 in case of the TP P/S on both medial and lateral side, which gives the TP P/S model the highest sliding-rolling value among the tested prostheses.

The BioMet Oxford model (Figure 16) has a very low sliding attribute between 20-60° of flexion angle at the medial side (it jumps to a higher value only for a very limited period), and beyond 60° it follows also a closely linear growth to 0.88 on the lateral side and 0.85 on the medial side. In contrast with the BioTech TP and the SZIU models, the curve is very smooth after 60° of flexion angle.

As for the kinetics, the forces have the same magnitude as the BioTech TP P/S, although here more scatter appears at the lateral side (see Figures 17 and 18).

While the evolutions of the sliding-rolling functions are somewhat similar regarding the SZIU, BioTech TP- TP P/S or BioMet Oxford models, the DePruy prosthesis (Figure 19) follows a completely different and unusual pattern. The curve is practically constant, with less than 5% of periodic deviation. The maximum value of the curve is registered at 23° of flexion angle at the medial side where it reaches for a short interval the value of one, which means complete sliding, then the function decreases to 0.75. The contact forces (see Figures 20 and 21) are similar to the Biomet Oxford model.

If we compare the magnitude of the lateral and medial sliding-rolling ratio, a slightly higher percentage of sliding can always be credited to the medial compartment. This difference is quite visible for the DePruy prosthesis while it is less obvious concerning the SZIU, BioTech and BioMet models.

This difference was also confirmed by the study of Wilson et al. [31]. From 0° to 5° of flexion angle the sliding-rolling ratio at the medial side was significantly higher (approximately 1.5-2 times) compared to the lateral side; between 5° and 10° was about 1-0.5 times and from 20° of flexion angle the difference stays in the range of 5-8%. Since in general the sliding-rolling ratio is slightly (5-8%) higher on the medial side, the medial results were plotted on the following Figures 22 and 23.

By fitting a second-order function on each medial sliding-rolling curve, and summarizing them in one graph, the following results are obtained (see Figure 22).

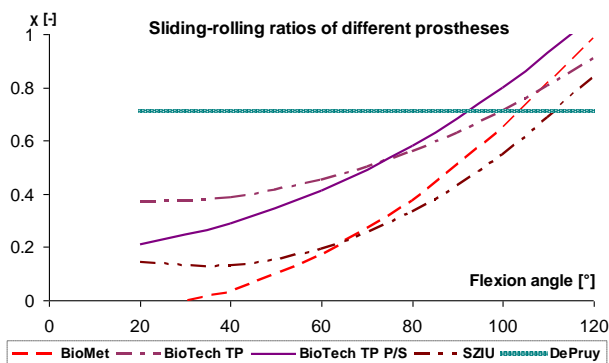


Figure 22

Summarized sliding-rolling ratios of the different models on the medial side

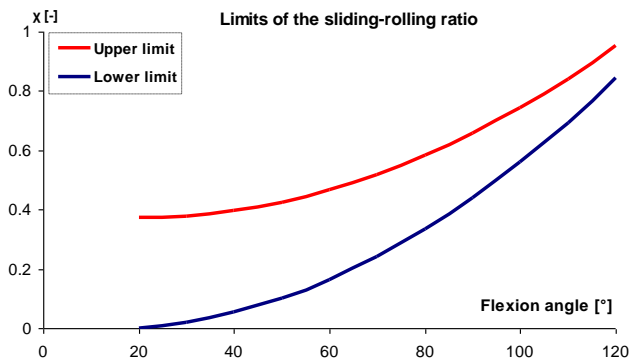


Figure 23

Limits of the sliding-rolling ratio on the medial side

From Figure 22, a well-visible trend appears along the flexion angle for the SZIU, BioTech TP, BioTech TP P/S and the BioMet Oxford models. In addition, upper and lower limit have been drawn where most of the functions are located (see Figure 23).

Conclusions

In this paper the evolution of the sliding-rolling ratio curves has been introduced in the active functional arc of the knee in the case of several commercial and one prototype prostheses. By these curves it becomes possible to estimate the applicable sliding-rolling ratio with respect to the flexion angle.

As was concluded by McGloughlin and Kavanagh [16], a higher sliding-rolling ratio generates a higher wear rate as well; thus, depending on the testing angle, a proper ratio has to be applied during tribological tests. Up to 50° of flexion angle 0.4-0.45 sliding-rolling ratio is adequate, as has been presented by earlier authors [10, 26, 27, 28]; above this specific angle, the currently determined sliding-rolling ratios are more prevalent, since at 120° of flexion angle the ratio can easily reach 0.85-0.95.

As a summary, the currently determined pattern (see Figures 22-23) – obtained by the five different prosthesis geometries – can provide a future limit for experimental tests related to the applicable sliding-rolling ratio with the actual normal and friction load. These applicable loads are represented in this study as normal and friction forces.

Acknowledgement

This work was supported by the FWO (project number: G022506), the Ghent University – Labo Soete, and the Szent István University – Faculty of Mechanical Engineering and Mechanical Engineering PhD School.

We would like to thank the useful comments of Prof. Gábor Krakovits in questions related to anatomy and prostheses.

References

- [1] Blunn G. W, Joshi A. B, Minns R. J.: Wear in Retrieved Condylar Knee Arthroplasties. *Journal of Arthroplasty*, **12** (1997), pp. 281-290
- [2] Braune W, Fischer O.: Bewegungen des Kniegelenkes, nach einer neuen Methode am lebenden Menschen gemessen. S. Hirtzel, Leipzig, Germany, 1891
- [3] Chittajallu S. K, Kohrt K. G.: FORM 2D – A Mathematical Model of the Knee. *Mathematical and Computer Modelling*, **24** (1999), pp. 91-101
- [4] Csizmadia B, Nádori E.: *Mozgástan (Dynamics)*, Nemzeti Tankönyvkiadó, Budapest, Hungary, 1997
- [5] Flannery M, McGloughlin T, Jones E, Birkinshaw C.: Analysis of Wear and Friction of Total Knee Replacements. Part I. Wear Assessment on a Three Station Wear Simulator. *Wear*, **265** (2008), pp. 999-1008
- [6] Freeman M. A. R.: How the Knee Moves. *Current Orthopaedics*, **15** (2001), pp. 444-450
- [7] Fregly B. J, Besier T. F, Lloyd D. G, Delp S. L, Banks S. A, Pandy M. G, D'Lima D. D.: Grand Challenge Competition to Predict in Vivo Knee Loads. *Journal of Orthopaedic Research*, **30** (2012), pp. 503-513

- [8] Gear C. W.: Simultaneous Solution of Differential-Algebraic Equations. *IEEE Transactions on Circuit Theory*, **18** (1971), pp. 89-115
- [9] Gyurecz Gy, Renner G.: Correcting Fine Structure of Surfaces by Genetic Algorithm. *Acta Polytechnica Hungarica*, **8** (2011), pp. 181-190
- [10] Hollman J. H, Deusinger R. H, Van Dillen L. R, Matava M. J.: Knee Joint Movements in Subjects without Knee Pathology and Subjects with Injured Anterior Cruciate Ligaments. *Physical Therapy*, **82** (2002), pp. 960-972
- [11] <http://www.biomet.hu>, Accessed: 03.04.2012
- [12] <http://www.biotech-medical.com>, Accessed: 02.28.2012
- [13] Iwaki A, Pinskerova V, Freeman M. A. R.: The Shapes and Relative Movements of the Femur and Tibia in the Unloaded Cadaver Knee. *Journal of Bone and Joint Surgery*, **82-B** (2000), pp. 1189-1195
- [14] Lauren M. P, Johnson T. S, Yao J. Q, Blanchard C. R, Crowninshield R. D.: In Vitro Lateral versus Medial Wear of a Knee Prosthesis. *Wear*, **255** (2003), pp. 1101-1106
- [15] Ling Z-K, Guo H-Q, Boersma S.: Analytical Study on the Kinematic and Dynamic Behaviors of the Knee Joint. *Medical Engineering and Physics*, **19** (1997), pp. 29-36
- [16] McGloughlin T, Kavanagh A.: The Influence of Slip Ratios in Contemporary TKR on the Wear of Ultra-High Molecular Weight Polyethylene (UHMWPE): An Experimental View. *Journal of Biomechanics*, **31** (1998), p. 8
- [17] Michalíková M, Bednarčíková L, Petřík M, Živčák J, Raši R.: The Digital Pre-Operative Planning of Total Hip Arthroplasty. *Acta Polytechnica Hungarica*, **7** (2010), pp. 137-152
- [18] Momersteeg T. J. A, Blankevoort L, Huiskes R, Kooloos J. G. M, Kauer J. M. G, Hendriks J. C. M.: The Effect of Variable Relative Insertion Orientation of Human Knee Bone-Ligament-Bone Complexes on the Tensile Stiffness. *Journal of Biomechanics*, **28** (1995), pp. 745-752
- [19] Mow V. C, Soslowsky L. J.: Lubrication and Wear of Joints. In: Mow V. C, Hayes W. C.: *Basic Orthopaedic Biomechanics*. Raven Press, New York, USA (1991), pp. 245-292
- [20] MSC.ADAMS Basic Full Simulation Package: Training Guide. Santa Ana, USA, 2005
- [21] Nägerl H, Frosch K. H, Wachowski M. M, Dumont C, Abicht Ch, Adam P, Kubein-Meesenburg D.: A Novel Total Knee Replacement by Rolling Articulating Surfaces. *In Vivo Functional Measurements and Tests. Acta of Bioengineering and Biomechanics*, **10** (2008), pp. 55-60
- [22] Pinskerova V, Johal P, Nakagawa S, Sosna A, Williams A, Gedroyc W, Freeman M. A. R.: Does the Femur Roll-Back with Flexion? *Journal of Bone and Joint Surgery*, **86-B** (2004), pp. 925-931
- [23] Quian S. H, Ge S. R, Wang Q. L.: The Frictional Coefficient of Bovine Knee Articular Cartilage. *Journal of Bionic Engineering*, **32** (2006), pp. 79-85

- [24] Reinholz A, Wimmer M. A, Morlock M. M, Schnelder E.: Analysis of the Coefficient of Friction as Function of Slide-Roll Ratio in Total Knee Replacement. *Journal of Biomechanics*, **31** (1998), p. 8
- [25] Saikko V, Calonius O.: Simulation of Wear Rates and Mechanisms in Total Knee Prostheses by Ball-On-Flat Contact in a Five-Station, Three Axis Rig. *Wear*, **253** (2002), pp. 424-429
- [26] Sukumaran J, Ando M, De Baets P, Rodriguez V, Szabadi L, Kalacska G, Paepegem V.: Modelling Gear Contact with Twin-Disc Setup. *Tribology International*, **49** (2012), pp. 1-7
- [27] Van Citters D. W, Kennedy F. E, Collier J. P.: Rolling Sliding Wear of UHMWPE for Knee Bearing Applications. *Wear*, **263** (2007), pp. 1087-1094
- [28] Van Citters D. W, Kennedy F. E, Currier J. H, Collier J. P, Nichols T. D.: A Multi-Station Rolling/Sliding Tribotester for Knee Bearing Materials. *Journal of Tribology*, **126** (2004), pp. 380-385
- [29] Van Ijsseldijk E. A, Valstar E. R, Stoel B. C, Nelissen R. G. H. H, Reiber J. H. C, Kaptein B. L.: The Robustness and Accuracy of in Vivo Linear Wear Measurements for Knee Prostheses Based on Model-based RSA. *Journal of Biomechanics*, **44** (2011), pp. 2724-2727
- [30] Wimmer M. A.: Wear of Polyethylene Component Created by Rolling Motion of the Artificial Knee Joint, Aachen, Shaker Verlag, Germany, 1999
- [31] Wilson D. R, Feikes J. D, O'Connor J. J.: Ligaments and Articular Contact Guide Passive Knee Flexion. *Journal of Biomechanics*, **31** (1998), pp. 1127-1136
- [32] Zuppinger H.: Die aktive im unbelasteten Kniegelenk. Wiesbaden, Germany, 1904

Nomenclature

$\chi(\alpha)$: Sliding-rolling ratio (-).

α : Flexion angle of the knee ($^{\circ}$).

$\bar{r}_{Ci}(t)$: Vector describing the path of the contact points (m).

$\bar{r}_{CMF}(t)$ and $\bar{r}_{CMT}(t)$: Displacement vectors of the center of masses (m).

$\bar{v}_{CMF}(t)$ and $\bar{v}_{CMT}(t)$: Velocity vectors of the center of masses (m/s).

$\bar{\omega}_{CMF}(t)$ and $\bar{\omega}_{CMT}(t)$: Angular velocity vectors of the center of masses (1/s).

$\bar{e}_{Ci}(t)$: Tangential unit-vector of the contact path (-).

$\bar{r}_{CF}(t)$ and $\bar{r}_{CT}(t)$: Displacement vectors determining the contact point with respect to the center of masses (m).

$\bar{v}_{CF}(t)$ and $\bar{v}_{CT}(t)$: Velocity vectors determining the velocities in the contact point with respect to the center of masses (m/s).

$v_{CFt}(t)$ and $v_{CTt}(t)$: Tangential velocity components in the contact point (m/s).

$v_{CFn}(t)$ and $v_{CTn}(t)$: Normal velocity components in the contact point (m/s).

$S_{femur}(t)$ and $S_{tibia}(t)$: Arc lengths of femur and tibia (m).